Structure-mechanical function relations at nano-scale in heat-affected human dental tissue

Sui, Tan; Sandholzer, Michael A; Le Bourhis, Eric; Baimpas, Nikolaos; Landini, Gabriel; Korsunsky, Alexander M

DOI:
10.1016/j.jmbbm.2013.12.014

JOURNAL OF THE MECHANICAL BEHAVIOR OF BIOMEDICAL MATERIALS 32 (2014) 113–124

Available online at www.sciencedirect.com

ScienceDirect

www.elsevier.com/locate/jmbbm

Research Paper

Structure-mechanical function relations at nano-scale in heat-affected human dental tissue

Tan Sui[a,*], *Michael A. Sandholzer*[b], *Eric Le Bourhis*[c], *Nikolaos Baimpas*[a], *Gabriel Landini*[b], *Alexander M. Korsunsky*[a]

[a]*Department of Engineering Science, University of Oxford, Parks Road, Oxford OX1 3PJ, United Kingdom*
[b]*School of Dentistry, College of Medical and Dental Sciences, University of Birmingham, St Chad's Queensway, Birmingham B4 6NN, United Kingdom*
[c]*Institut P',CNRS UPR 3346, University of Poitiers, SP2MI, BP 30179, F86962 Futuroscope Chasseneuil Cedex, France*

ARTICLE INFO

Article history:
Received 15 August 2013
Received in revised form
30 November 2013
Accepted 14 December 2013
Available online 20 December 2013

Keywords:
Dental tissue
Thermal treatment
SAXS/WAXS
Nanoindentation
Mechanical-structural correlation

ABSTRACT

The knowledge of the mechanical properties of dental materials related to their hierarchical structure is essential for understanding and predicting the effect of microstructural alterations on the performance of dental tissues in the context of forensic and archaeological investigation as well as laser irradiation treatment of caries. So far, few studies have focused on the nano-scale structure-mechanical function relations of human teeth altered by chemical or thermal treatment. The response of dental tissues to thermal treatment is thought to be strongly affected by the mineral crystallite size, their spatial arrangement and preferred orientation. In this study, synchrotron-based small and wide angle X-ray scattering (SAXS/WAXS) techniques were used to investigate the microstructural alterations (mean crystalline thickness, crystal perfection and degree of alignment) of heat-affected dentine and enamel in human dental teeth. Additionally, nanoindentation mapping was applied to detect the spatial and temperature-dependent nanomechanical properties variation. The SAXS/WAXS results revealed that the mean crystalline thickness distribution in dentine was more uniform compared with that in enamel. Although in general the mean crystalline thickness increased both in dentine and enamel as the temperature increased, the local structural variations gradually reduced. Meanwhile, the hardness and reduced modulus in enamel decreased as the temperature increased, while for dentine, the tendency reversed at high temperature. The analysis of the correlation between the ultrastructure and mechanical properties coupled with the effect of temperature demonstrates the effect of mean thickness and orientation on the local variation of mechanical property. This structural–mechanical property alteration is likely to be due to changes of HAp crystallites, thus dentine and enamel exhibit different responses at different temperatures. Our results enable an improved understanding of the mechanical properties correlation in hierarchical biological materials, and human dental tissue in particular.

*Corresponding author. Tel.: +44 18652 83447; fax: +44 18652 73010.
E-mail address: tan.sui@eng.ox.ac.uk (T. Sui).

1751-6161/$ - see front matter © 2013 Elsevier Ltd. All rights reserved.
http://dx.doi.org/10.1016/j.jmbbm.2013.12.014

1. Introduction

The bulk of human teeth consists of two main mineralised tissues, collagen-rich dentine and highly mineralised enamel. They join forming a complex and mechanically durable dentine–enamel junction (DEJ) that contributes to the life-long success of the tooth structure under thermo-mechanical loadings encountered in the oral cavity under the conditions such as mastication, chemically active environment and thermal shock (He and Swain, 2009; Marshall et al., 1998; Ten Cate, 1998). This remarkable performance provides the motivation for numerous investigations into the detail of the micro- and nano-structure of enamel, dentine and the DEJ. The knowledge of the mechanical properties related to the hierarchical structure of dentine, enamel and the DEJ is essential for understanding and predicting the effects of microstructural alterations due to disease, treatment, or environmental or thermal exposure on the performance of dental tissues and their artificial replacements.

The use of advanced high-energy techniques is increasing in modern dentistry. With the advent of a variety of new laser systems spanning by a range of energy densities and pulse durations, clinical treatments such as laser-assisted caries protection were proposed and developed. Local temperature induced by laser as high as 1000 °C may be achieved during laser treatment (Fried et al., 2002; Zuerlein et al., 1999). Improved caries prevention is surmised to be associated with increased mineralisation and HAp crystallite sintering that leads to the sealing of dentinal tubules. However, the confirmation of this by direct microscopic characterisation of the very thin surface layer affected by laser therapies is an extremely challenging experimental task. In addition, in the context of archaeological and forensic investigations, the macroscopic alterations (e.g. surface colour) can be used to deduce an approximate temperature range, while the investigation of the micro- and ultrastructural alterations of skeletal hard tissues exposed to high temperatures turned out to be an excellent means of obtaining reliable estimates of the temperatures of exposure (Piga et al., 2009; Thompson, 2005; Thompson et al., 2011). The above considerations provide a strong motivation for a detailed study into the effect of thermal exposure on the nano-structure properties of human dental tissue. In order to understand and quantify more precise information about the evolution of the hierarchical nano/micro-structure under in situ thermal exposure, the application of advanced non-destructive techniques offers an appropriate route.

Synchrotron based X-ray diffraction, small- and wide angle X-ray scattering (SAXS and WAXS, respectively), are advanced non-destructive techniques that enable characterising the ultrastructure, mechanical property and texture evaluation of mineralised tissues (Al-Jawad et al., 2007; Daniels et al., 2010; Deymier-Black et al., 2010). WAXS (XRD) has been proved to be capable of showing the distinct differences of HAp of animal and human bone mineral upon heating (Beckett et al., 2011; Piga et al., 2008; Piga et al., 2013; Rogers et al., 2010), however most lab-based XRD usually involves the mechanical destruction of a sample and estimation of a subsequent volume-weighted averaged result, without providing local fine-scale changes of ultrastructure (Hiller et al., 2003). Compared with conventional high-magnification microscopic methods, SAXS allows a far higher throughput of samples with shorter time of analysis and non-destructive identification of local structural alterations at the nano-scale. However, the investigation of thermal treated mineralised tissues using SAXS technique is still lacking, and only recently, lab-based SAXS was used to characterize the structural changes in human bone for forensic and archaeological purposes (Hiller et al., 2003), but few in the corresponding SAXS data analysis on human dental tissues in particular.

Nanoindentation has recently emerged as a powerful tool for measuring the nano-scale mechanical properties in biomaterials (Ebenstein and Pruitt, 2006). Nanoindentation in mineralised tissues have been extensively studied and reviewed by Kinney et al. (Kinney et al., 2003) and Haques et al. (Haque, 2003). In teeth, a primary focus has been to map mechanical properties across the normal dental tissues to understand the role of local properties and hierarchical structure, and has also been coupled with chemical mapping (Fong et al., 2000; Marshall et al., 2001; Roy and Basu, 2008). However, to date, no studies have been reported on the investigation of the variation of mechanical properties on thermally treated dental tissues. Tesch et al. (Tesch et al., 2001) successfully applied SAXS and nanoindentation to characterize non-treated dentine and observed variations of mechanical and structural properties in correlations but the resolution is low. In the present investigation of heat-induced alterations of hard dental tissues with high resolution, a SAXS mapping setup was combined with nanoindentation mapping. The results obtained here are likely to help in a better understanding of the internal architecture alterations and hierarchical properties changes due to heat exposure. In addition, the effect of exposure of human skeletal hard tissues to high temperatures is an important topic of study in the context of forensic investigations and archaeological analysis (Beckett et al., 2011; Enzo et al., 2007; Piga et al., 2009; Rogers and Daniels, 2002; Shipman et al., 1984).

The aim of this study was to have a medium resolution mapping using synchrotron-based SAXS/WAXS technique to characterise the structural features both in dentine and enamel, as well as in the region near the DEJ of human teeth samples with various thermal treatments in order to analyse the ultrastructural variation (mean crystalline thickness, crystal perfection, orientation and degree of alignment) and their correlation with the reduced modulus and hardness properties (measured by nanoindentation).

2. Materials and methods

2.1. *Sample preparation*

Four freshly extracted intact human molars (ethical approval obtained from the National Research Ethics Committee; NHS-REC reference 09.H0405.33/ Consortium R&D No. 1446) were disinfected in 15 mM sodium azide solution and washed under running water for 5–6 h before mechanically cleaned to eliminate residues. Teeth were excluded from the study

because of damage (e.g. broken roots), endodontic treatment, dental restorations or caries. Details such as age, sex and patients ethnic background remained anonymous as part of patient confidentiality regulations. In total, twelve teeth sections ($3 \times 1 \times 0.5\ mm^3$) were prepared and kept in a hydrated state in Phosphate Buffer Solution (PBS) at 4 °C before the experiment (Marten et al., 2010). Of these, 10 sections were allocated into five temperature groups for 30 min constant exposure at 400 °C–800 °C (in steps of 100 °C), and two additional unheated sections were used as controls. An ashing furnace (Carbolite AAF 11/3, Sheffield, United Kingdom) was used to generate the thermal treatment. Each tooth sample was then subjected to a thermal history that heated the sample to the final (maximum) temperature (constant exposure) and were then removed from the furnace after the desired duration of exposure was reached, and subsequently cooled down in the crucibles to room temperature and stored in padded containers.

For the purpose of planning the measuring positions and Region of Interests (ROIs) of the SAXS/WAXS mapping, micro-CT scans of the samples were performed with a SkyScan 1172 scanner (SkyScan, Kontich, Belgium) at 1.9 μm resolution using 80 kV voltage, 120 μA current and a 0.5 mm Aluminium filter (Fig. 2a–c). The resulting data were reconstructed with SkyScan NRECON package and subsequent models were recreated with Fiji imaging software (Eliceiri et al., 2012). In addition, it should be noted that the micro-CT scan was also used on the selection of samples in order to largely guarantee that the DEJ plane of the selected samples was almost parallel to the X-ray beam.

The nanoindentation measurements were performed on the same teeth sections after embedding in Epoxy resin (Buehler Epo-Kwick, Buehler Ltd., Lake Bluff, IL) to preserve their integrity and were analysed in the dry condition. The maximum peak temperatures of the epoxy during curing the manufacturer is 145 °C with a short period of time, which the influence on the sample is thought to be limited. Furthermore, the sections are carefully ground with a series of grinding papers (P800-P4000) to expose the surface and finally polished with 3 μm diamond polishing compound. This way, it was made sure that properties of the tissue were measured, and not properties of the epoxy resin.

In summary, six samples (RT, 400 °C, 500 °C, 600 °C, 700 °C and 800 °C) were used for the SAXS/WAXS mapping measurements and three out of those six samples including RT, 500 °C and 700 °C were further selected for the nano-indentation mapping, since these temperatures were representatives of major compositional changes and weight loss (Pramanik et al., 2013).

2.2. Micro-focus small angle X-ray scattering experiment

Micro-focus SAXS experiments were performed on the I22 beamline at Diamond Light Source (DLS, Oxford, UK) using monochromatic 18 keV X-rays. The distance between detector and sample was 1040 mm, guaranteeing that clear and complete SAXS patterns and a partial WAXS pattern could be captured on the 2D detector (Pilatus 2 M, Dectris Ltd., Baden, Switzerland) positioned downstream of the sample. The use of the incident X-ray beam focused down to the spot size of $14.5 \times 19\ \mu m^2$ allowed the achievement of the required spatial resolution. Each sample was mounted upright in air and scattering patterns were collected in transmission mode while the sample was repeatedly shifted in the plane perpendicular to the X-ray incident beam travelling in the z-direction to collect the map of SAXS patterns. The mapping area of region of interest (ROI) for the control sample and samples from 400 °C to 800 °C was $0.6 \times 0.6\ mm^2$. The spacing between each two measurement points of the mapping scans was 40 μm both in longitudinal (y-direction) and transverse (x-direction) directions, resulting in a total of 225 scattering patterns per sample (see Fig. 1a).

The experiment allows us to consider the DEJ a functionally and structurally gradient layer – a common approximation that is used with considerable success in the study of inhomogeneous materials, interfaces, surface treated systems, etc. Since the main interest is in-plane variation, therefore, all possible efforts have been made to ensure that the X-ray beam travelling through the sample is close to parallel to the DEJ and the beam size ($14.5 \times 19\ \mu m^2$) is able to provide a result averaged over the gauge volume that moves across the DEJ. Samples of the thickness ~500 μm represent the practical limit in terms of survival of thermal exposure. As for the SAXS measurements conducted in transmission mode in these experiments, sample thinner than that is likely to result in low intensity of the SAXS signal.

2.3. Scattering data analysis

2.3.1. SAXS

Quantitative interpretation of SAXS patterns provides insight into the mean thickness, orientation and degree of alignment of dense particles. For initial quantitative analysis, 2-D diffraction images were converted into 1-D intensity profiles and pre-processed using the Fit2D software package (Hammersley, 1997).

a) Mean crystalline thickness
The scattering intensity $I(q, \varphi)$ was radially integrated over the entire range of the azimuthal angle φ to obtain a function of $I(q)$, where q represents the scattering vector. The crystal mean thickness T is defined as the *Porod* chord length based on *Porod's law* valid in a two-phase system

$$T = \frac{4}{\pi \frac{Q}{P}} \quad (1)$$

where P is the *Porod* constant given by $I(q) = Pq^{-4}$ (*Porod's law* at large q range), which can be determined from the $Iq^4 \sim q^4$ plot, and Q is the integrated area of the $Iq^2 \sim q$ plot. Note that the definition of T was used without any assumption of the particle shape. However, for specific cases of needle or platelet shape, T can be interpreted as an average measurement of the smallest dimension of crystallites. The actual mean crystalline thickness can be further calculated based on T and other factors like volume fraction (Fratzl et al., 1996).

b) Orientation and degree of alignment
The degree of alignment (ρ) of HAp crystalline particles is used to describe the percentage of aligned particles. To quantify it as well as the preferred orientation, the SAXS

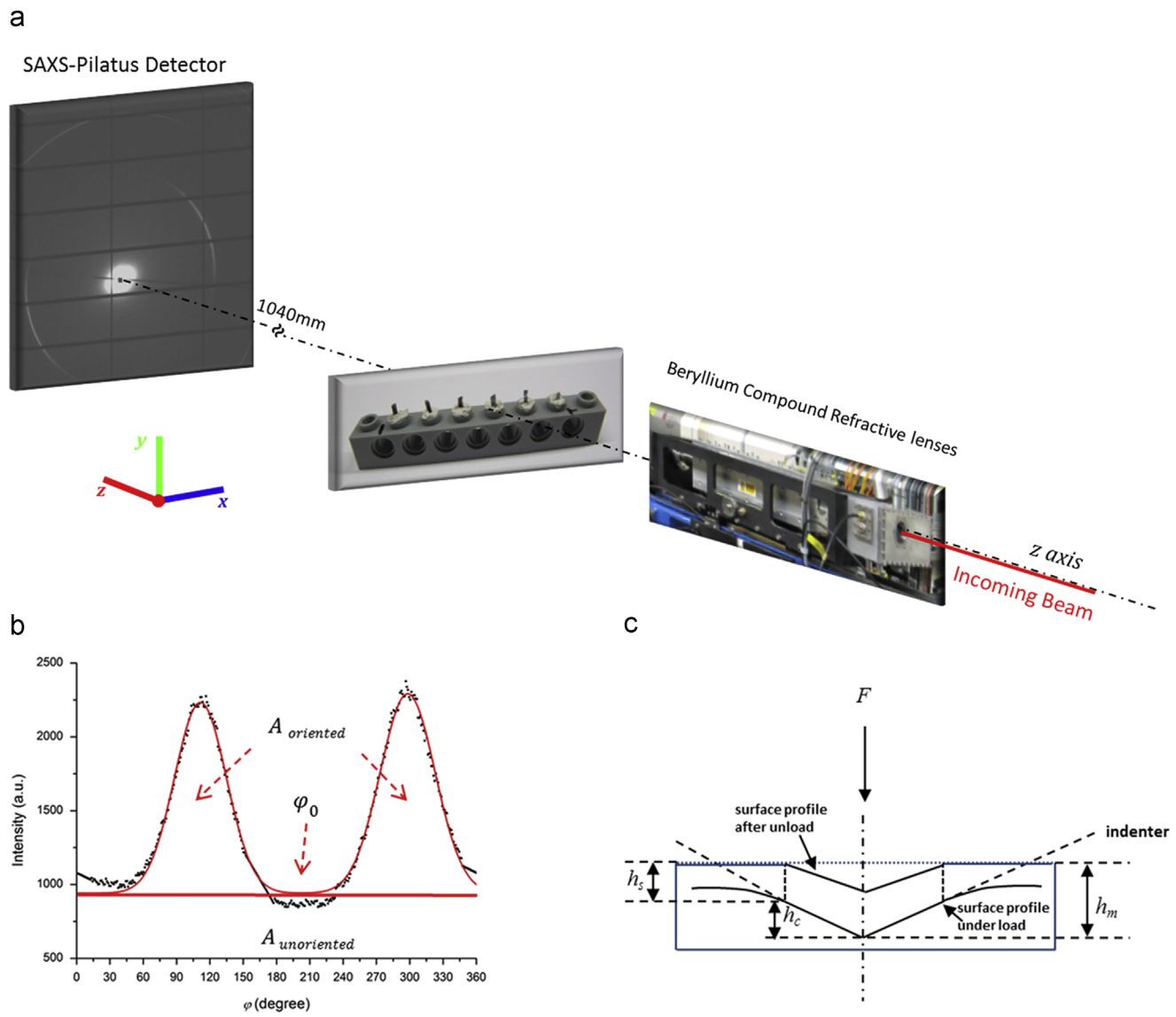

Fig. 1 – Schematic diagram of the experimental setup. (a) micro-focus SAXS setup, WAXS patterns can also be partly obtained on the SAXS-Pilatus detector, (b) A plot of the integrated curve $I(\varphi)$ (black points). The Gauss fit is also shown in the figure (red line). The predominant orientation φ_0 is the average position of the two peaks. The ratio $A_{oriented}/(A_{oriented}+A_{unoriented})$ gives the degree of alignment and (c) nanoindentation profile showing the quantities used in the analysis. (For interpretation of the references to color in this figure legend, the reader is referred to the web version of this article).

patterns were integrated over all the available scattering vectors q, resulting in a function $I(\varphi)$ with the azimuthal angle φ (Rinnerthaler et al., 1999; Tesch et al., 2003), which is shown in Fig. 1b. The Gauss fit is also shown in the figure (red line). In the plot of $I(\varphi)$, the average position of the two peaks determines the predominant orientation φ_0, and the degree of alignment is defined as the ratio

$$\rho = \frac{A_{oriented}}{A_{oriented} + A_{unoriented}} \quad (2)$$

where $A_{unoriented}$ is the area of the constant background level and $A_{oriented}$ is the overall area under the curve of $I(\varphi)$ subtracting the background. The value of the degree of alignment ranges from 0 to 1, where $\rho = 0$ indicates no predominant orientation within the plane of the section and $\rho = 1$ indicates a perfect alignment of all crystallites (Rinnerthaler et al., 1999; Tesch et al., 2003).

2.3.2. WAXS

WAXS patterns are represented by separated diffraction rings, containing characteristic information related to the crystal structure. The analysis of WAXS patterns is performed using the *Bragg's law*, which establishes the relationship between the spacing of atomic planes in crystals and the scattering angle at which these planes produce intense reflections (Bragg and Bragg, 1933). The (002) lattice plane reflection ring from HAp contains the information on the orientation of the c-axis of the crystals as well as the fibril orientation due to their parallel orientation, which is strong

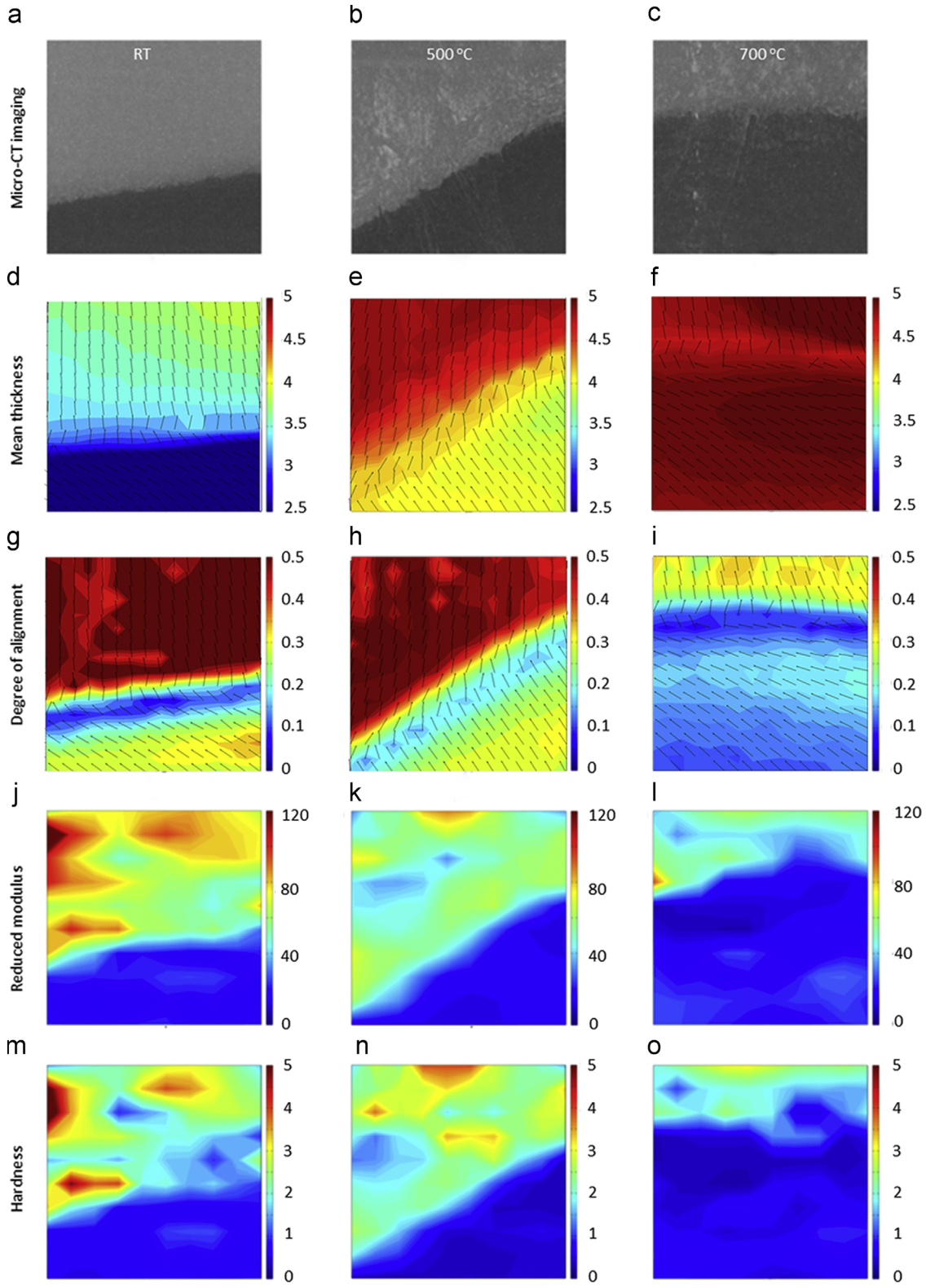

Fig. 2 – Region of interest (0.6 × 0.6 mm^2) of dental slice mapped with SAXS and nanoindentation techniques. Each column represents the results within the same area under a certain temperature as labelled. (a–c) ROI of RT (room temperature), 500 °C and 700 °C samples revealed by Micro-CT; 2D colour coded of SAXS results: (d–f) mean thickness (nm) and (g–i) degree of alignment of HAp crystallites, with the crystal orientation marked by the black lines. The mean thickness of the crystallites in both dentine and enamel increases as the temperature increases (from light blue to red for enamel and from dark blue to red for dentine). However, the spatial difference between dentine and enamel decreases with temperature. The degree of alignment drops as the temperature increases (from red to yellow for enamel and from yellow to blue for dentine); 2D colour coded of nanoindentation results: (j–l) reduced modulus (GPa) and (m–o) hardness (GPa); The reduced modulus and hardness of enamel is observed to decrease significantly with the increasing temperature (from yellow–red mixture to light blue). (For interpretation of the references to color in this figure legend, the reader is referred to the web version of this article).

and distinct (Deymier-Black et al., 2010) Therefore, only the (002) peak of interest is selected for interpretation.

2.4. Nanoindentation experiment

A nanohardness tester (NHT) with a Berkovich diamond probe from CSM (CSM, Neuchatel, Switzerland) was utilised to perform nanoindentation on the thermally treated samples. The calibration was done by fused silica and the procedure suggested by Oliver and Pharr (Oliver and Pharr, 1992) was used to correct for the load-frame compliance of the apparatus and the imperfect shape of the indenter tip. The tests were performed at room temperature under force control feedback mode to a peak force of 2 mN. A load function composed of 30 s loading, followed by 30 s holding and 30 s unloading was used (Le Bourhis et al., 2004; Patriarche et al., 2004). The hold period at maximum load (30 s) is used to limit creep upon unloading, and thereby allow for a more reliable extraction of mechanical properties from the unloading curve (Angker et al., 2005). The contact depth was between 100 and 400 nm that is much lower than the tooth sample thickness (0.5 mm), so that the properties obtained can be confidently assigned to the bulk. Maps of indents were performed along the same ROI used for the scattering experiment. The indents were spaced approximately 60 μm apart both in the x- and y-directions and performed using automation.

Nanoindentation tests are widely used to determine some material properties. Every nano-indent operation involves a loading and unloading process, and the indentation load-depth data is recorded for each operation (Hsu et al.). A schematic diagram of nanoindentation process (Fig. 1c) is shown, where indentation depth h is the summation of h_s (displacement due to elastic deformation) and h_c (contact depth). S is the contact stiffness at maximum penetration and is the initial slope of the unloading curve. Using the compliance method, the hardness H and reduced modulus E_r can be determined directly from analysis of load-displacement data (Ebenstein and Pruitt, 2006). The hardness of the sample can be obtained by dividing the load by the projected area of indentation

$$H = \frac{F_m}{A_c} \tag{3}$$

where A_c ($A_c = 24.5h_c^2$ for a perfect tip) is the contact area, F_m is the force at maximum load. The composite modulus E^* (sample and diamond) is extracted from

$$\frac{1}{E^*} = \frac{2\beta}{S}\sqrt{\frac{A_c}{\pi}} \tag{4}$$

where β is a correction factor depending on the rip geometry ($\beta = 1.034$ for a Berkovich one). The relation with diamond and sample properties is given by

$$\frac{1}{E^*} = \frac{1-\nu_D^2}{E_D} + \frac{1-\nu_S^2}{E_S} \tag{5}$$

where E and ν are Young's modulus and Poisson ratio and the subscripts D and S are for diamond and sample respectively ($E_D = 1141$ GPa, $\nu_D = 0.07$). The reduced modulus is referred to as

$$\frac{1}{E_r} = \frac{1-\nu_s^2}{E_s} \tag{6}$$

which is reported in (Le Bourhis and Patriarche, 2007; Lim et al., 2005; Oliver and Pharr, 1992).

2.5. Statistical analysis

The calculated mean crystalline thickness values were statistically analysed with two-tailed paired sample t-tests using SPSS version 19 (IBM SPSS Inc., Chicago, USA). Probability levels of $p < 0.05$ (95% confidence interval) were considered statistically significant.

3. Results

Colour coded 2D mapping provides a general qualitative understanding of the spatial distribution of the ultrastructural and mechanical properties and their variations with temperature. It also offers a validation on extracting the line measurements or 1D plot with the detailed quantitative information of the changes and correlation of the results. For reasons of consistency, the central line values were chosen in all samples and no dependency of the measurement results on the line position was found. In this section, both the 2D mapping results and the line plot were presented.

3.1. Ultrastructural observations

3.1.1. Mean crystalline thickness

The spatial mean thickness variations of HAp crystallites in the control sample (RT, room temperature), samples heat treated at 500 °C and 700 °C were visualized in Fig. 2d–f as colour coded 2D-plot. Similar features from the three samples were observed, of which the mean crystalline thickness decreased from enamel to DEJ, and further down through deeper dentine. From Fig. 2d–f, it was found that the mean thickness of HAp crystallites increases with temperature, which was reflected through the 2D colour changes (enamel from blue in Fig. 2d to red in Fig. 2f, while dentine from dark blue to red). In addition, the spatial difference of the crystalline thickness between enamel and dentine was found to gradually decrease with temperature since in Fig. 2f, enamel and dentine almost shared the same colour.

In order to trace the average mean crystalline thickness alteration with increasing temperature, the thickness values along the central line of dentine and enamel in the mapping area were extracted from the 2D mapping results, which are shown in Fig. 3a. The variation of the averaged mean crystalline thickness of the central line of dentine and enamel with increasing temperature are illustrated in Fig. 4a and b, from which the crystallites in dentine is nearly tripled from 1.94 (SD: 0.06) nm at room temperature (RT) to 5.16 (SD: 0.06) nm at 800 °C, while that of crystallites in enamel increased from 3.81 (SD: 0.28) nm at RT to 4.90 (SD: 0.04) nm at 800 °C (for additional values see Table 1).

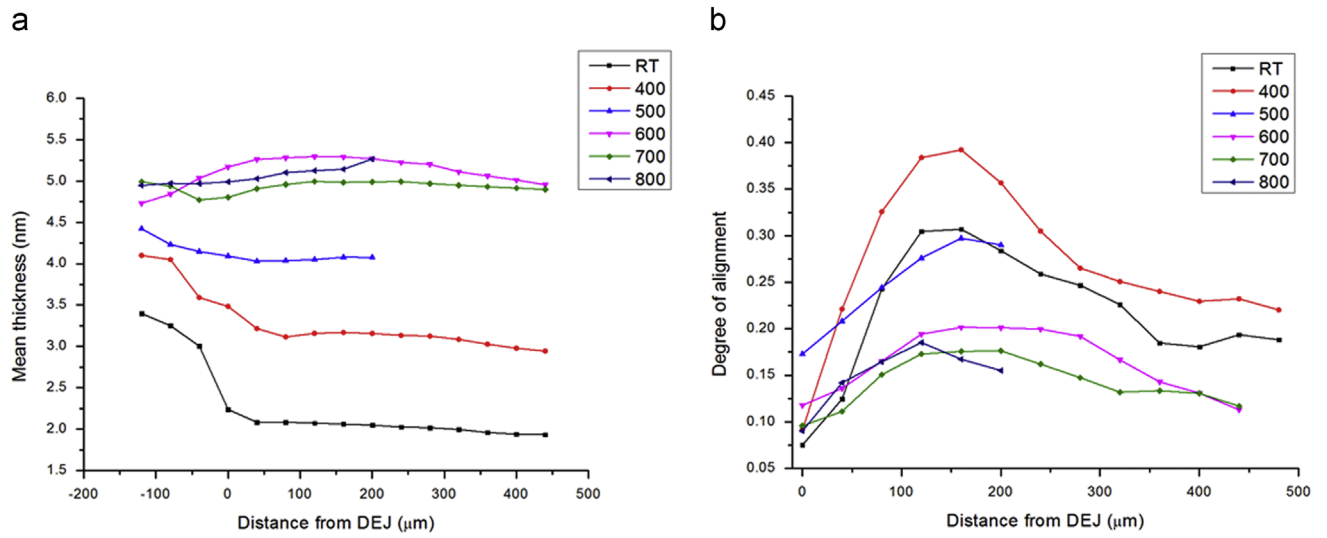

Fig. 3 – Ultrastructural variations along the central line from the 2D mapping result of ROI as a function of temperature and distance from DEJ. (a) results of the mean thickness of HAp. The first three measurement points (with minus distances from DEJ) represent the results in enamel; (b) results of the degree of alignment of HAp. Only the results of crystals in dentine are shown due to the complex variation happened beneath the DEJ.

3.1.2. *Orientation and degree of alignment*

The 2D maps of the degree of alignment variation of the same three samples (RT, 500 °C and 700 °C) within the interested region were shown respectively in Fig. 2g–i. The enamel and dentine show distinctive results visualized by the colour coding. Similar gradient features as the mean thickness results were observed. Generally, enamel has higher degree of alignment than dentine. However, it was found that the degree of alignment of both enamel and dentine decreased with temperature as the colour changed mostly from red to yellow in enamel and yellow to blue in dentine.

The angular orientation of the mineral particles in the 2D teeth slices is depicted by the small black lines superimposed on the degree of alignment mapping (shown in Fig. 2g–i). In enamel, all the particles are almost orthogonal to the DEJ plane. Same features can be observed for the particles in dentine but only for the region far beneath the transition area of the DEJ. It appears that mineral particles gradually become parallel to the DEJ plane through the region near DEJ.

The same central line of dentine and enamel as presented in the mean thickness visualization were selected from 2D mapping results. Only the line variation of the result in dentine is of the most interest and is shown in Fig. 3b. It is found that in the specific area in dentine just beneath the DEJ, the degree of alignment is relatively higher than the area far away from DEJ, shown as a bump in Fig. 3b. However, the overall degree of alignment of crystals in dentine decreased (also see Fig. 4c and d) and the bump gradually disappeared with increasing temperature. This indicates a tendency towards more random distribution of crystals as the temperature increased (see Table 1).

3.2. *Mechanical properties characterization*

3.2.1. *Reduced modulus*

Fig. 2j–l demonstrate the results of the spatial distribution of reduced modulus within the 2D interested area of the three samples (RT, 500 °C and 700 °C). The DEJ is clearly visible whereas the distribution inside the enamel and dentine is limited. It was found that only enamel has a pronounced colour change (from yellow–red in Fig. 2j to light blue in Fig. 2l), indicating a significant decrease of reduced modulus in enamel with temperature.

The variations of the averaged reduced modulus of the central line of dentine and enamel with respect to all the tested temperatures are illustrated in Fig. 4a and c. From the figure, it is found that the averaged reduced modulus of dentine decreased from 20 (SD: 6) GPa at RT to 15 (SD: 2) GPa at 500 °C and then increased to 29 (SD: 10) GPa at 800 °C, while in enamel it decreased from 70 (SD: 17) GPa at RT to 56 (SD: 17) GPa at 500 °C, and then further down to 47 (SD: 18) GPa at 800 °C (see Table 1).

3.2.2. *Hardness*

The overall spatial distribution of hardness of the three samples (RT, 500 °C and 700 °C) in the ROI can be observed in Fig. 2m–o. The DEJ is still recognisable, but the spatial changes are not as clearly shown as in the structural mapping of thickness and degree of alignment. Similar tendency as the reduced modulus was found that the hardness of enamel dropped significantly with temperature, which is reflected from the pronounced colour change.

The detailed alteration of the hardness with increasing temperature is also reflected in the variation of the averaged hardness of the selected central line of dentine and enamel (Fig. 4b and d). It was found that the averaged hardness variations have the similar tendency of variation as that of the averaged reduced modulus both in dentine and enamel. The averaged hardness in dentine decreased from 0.7 (SD: 0.1) GPa at RT down to 0.4 (SD: 0.1) GPa at 500 °C and then increased to 0.8 (SD: 0.3) GPa at 800 °C, while in enamel the averaged hardness decreased from 3.0 (SD: 1.3) GPa at RT to

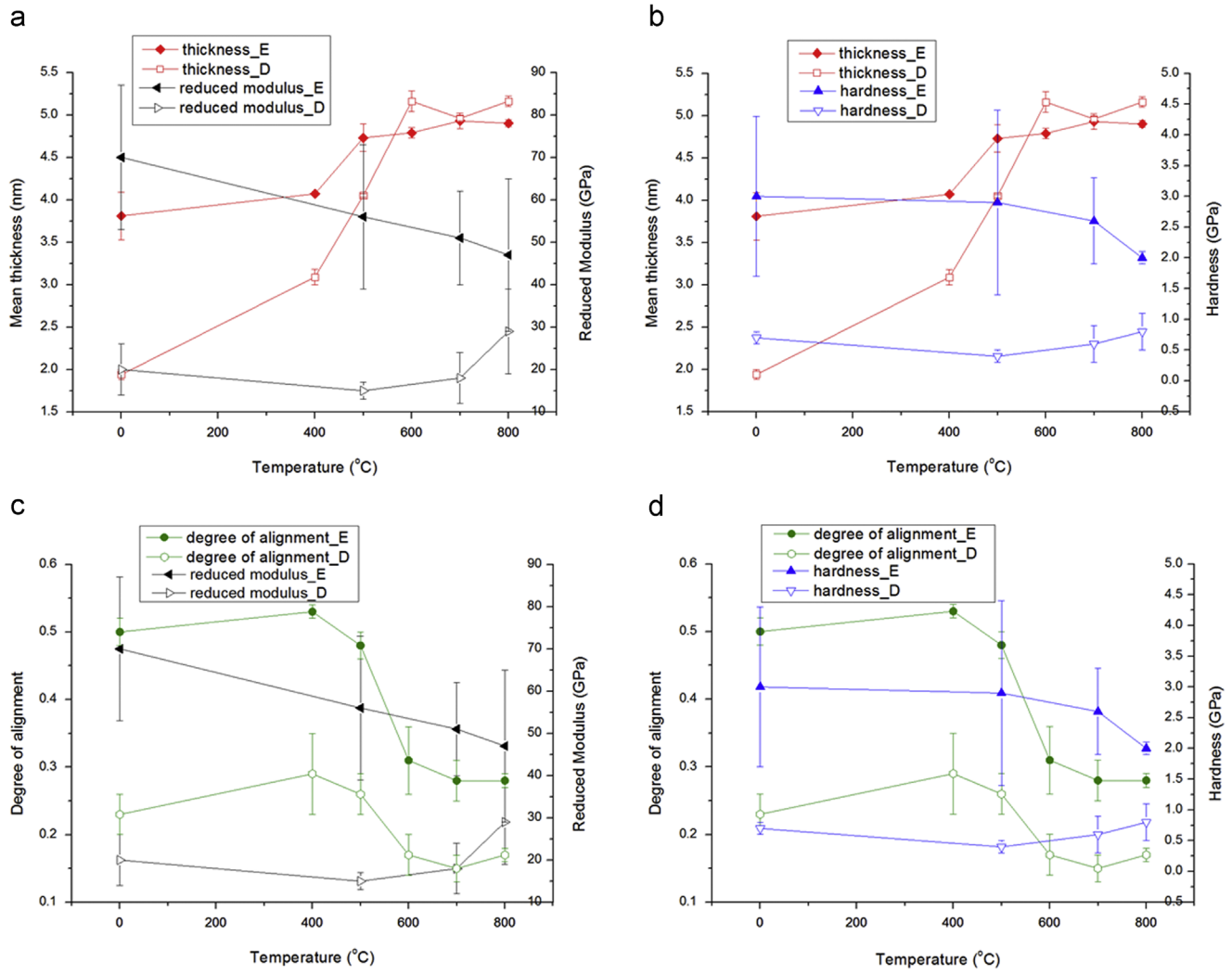

Fig. 4 – Correlation analysis between structural–mechanical parameters coupled with increasing temperature ("E" means enamel while "D" means dentine). All the results are the averaged values of different regions along the selected central line in ROI. (a) mean thickness vs. reduced modulus; (b) mean thickness vs. hardness; (c) degree of alignment vs. reduced modulus; (d) degree of alignment vs. hardness. Error bars ±1 SD. (For interpretation of the references to color in this figure, the reader is referred to the web version of this article).

Table 1 – Overview of SAXS and nanoindentation measurement results collected from central line from 2D mapping results. Statistical significance was evaluated using two-tailed paired sample *t*-tests with a 95% confidence interval for the mean thickness results (*$p<0.05$, **$p<0.005$, ***$p<0.0005$).

Temperature (°C)		Mean crystalline thickness (nm)	Degree of alignment	Hardness (GPa)	Reduced modulus (GPa)
RT	Enamel	3.81(SD: 0.28)	0.50(SD: 0.02)	3.0(SD: 1.3)	70(SD:17)
400		4.07(0.02)	0.53(0.01)		
500		4.73(0.16)*	0.48(0.02)	2.9(1.5)	56(17)
600		4.79(0.06)	0.31(0.05)		
700		4.93(0.09)	0.28(0.03)	2.6(0.7)	51(11)
800		4.90(0.04)	0.28(0.01)	2.0(0.1)	47(18)
RT	Dentine	1.94(0.06)	0.23(0.03)	0.7(0.1)	20(6)
400		3.09(0.09)***	0.29(0.06)		
500		4.05(0.02)***	0.26(0.03)	0.4(0.1)	15(2)
600		5.16(0.12)***	0.17(0.03)		
700		4.96(0.03)***	0.15(0.02)	0.6(0.3)	18(6)
800		5.16(0.06)	0.17(0.01)	0.8(0.3)	29(10)

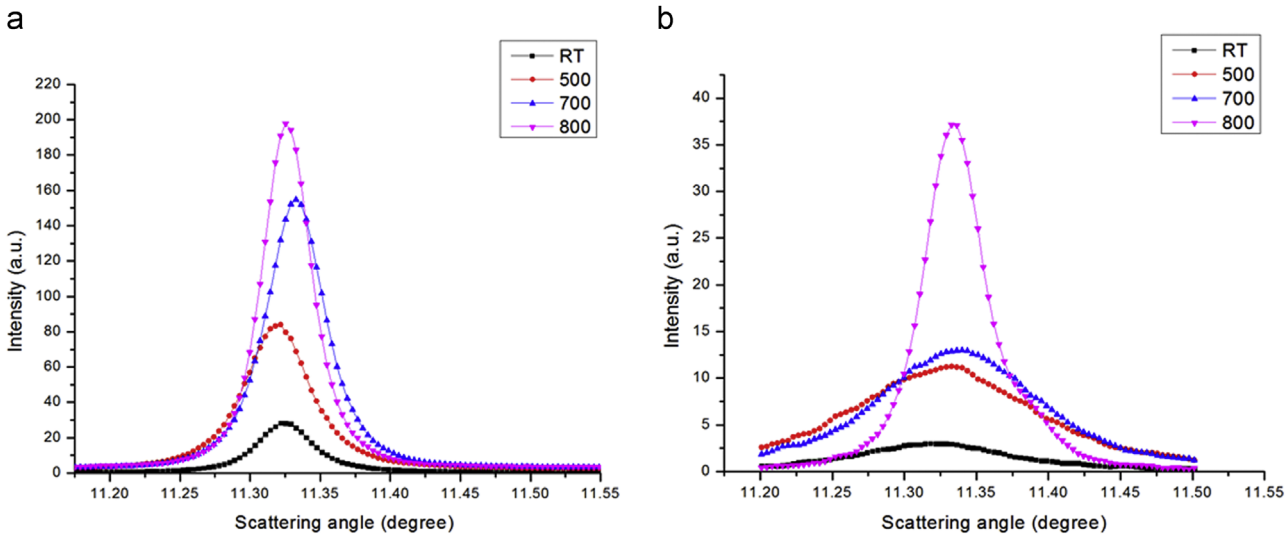

Fig. 5 – Intensity variation of the (002) reflection in the WAXS patterns of different regions at different temperatures: (a) enamel and (b) dentine. The observed peak sharpening and higher intensity at higher temperatures compared with the control sample indicates an increased diffraction contribution from HAp crystallites.

2.9 (SD:1.5) GPa at 500 °C and then to 2.0 (SD:0.1) GPa at 800 °C (see Table 1).

3.3. *Crystal perfection*

The WAXS patterns diffracted from HAp crystals in both the enamel and dentine provide information about the crystalline perfection difference in different regions. Due to the limited size of the 2D detector, only the (002) peak could be captured and analyzed. Fig. 5 shows the diffraction intensity variation of (002) peak for a selected region of scattering angles (11.2°–11.5°) with the temperature change. A sharpening of the peak at higher temperatures was observed, compared to the broad one of the control sample at lower temperature. This represents an increased diffraction contribution from HAp crystals within this scattering angle range as the temperature increased, which indicates that the crystal perfection increased remarkably during the heating. Note that the peak sharpening in dentine is more obvious than that in enamel.

4. Discussion

The ultrastructural alteration of skeletal hard tissues exposed to the thermal treatment process developed in the present study provides a better, more reliable basis for deducing the heating history, compared with the conventional methods based on monitoring the macro- and microstructural colour (Piga et al., 2009; Thompson, 2005; Thompson et al., 2013) in the forensic and archaeological investigation. In the clinical application like caries prevention, the present study offers an opportunity to characterise the microstructural features affected by laser therapies.

The previous analysis of the entire powdered tooth analysis obscures the sharpness of ultrastructural variations in dentine and enamel (Kugler, 2003; Piga et al., 2009). The present study clearly illustrates how the observed evolution of ultrastructure reflects the differences between dentine and enamel, suggesting that enamel and dentine must be investigated separately in order to evaluate the exposure temperature precisely in the forensic cases as well as optimise laser-assistant treatment in clinical application.

The structural–mechanical properties correlation to the temperature provides an additional guidance to track the heating history in the forensic study. In addition, for caries prevention, it provides the evidence that the alteration of mechanical properties should also be taken into account during the sintering process, since the decreased hardness may induce micro-cracks with increasing temperature.

4.1. *Ultrastructural observations*

4.1.1. *Mean crystalline thickness*

Overall the mean crystalline thickness distribution in dentine was more uniform compared with that in enamel. The mean crystalline thickness was observed to obviously decrease in enamel and slightly increase in dentine towards DEJ at low temperature, which may be ascribed to the gradient properties of human dental slice (Jacobs et al., 1973) as illustrated in Fig. 3a. However, as temperature increases, this gradient becomes smaller, which can be clearly seen in Fig. 3a. Besides the visible gradient features, the major drop was visible near the transition area around the DEJ, indicating the spatial structural variation in the human dental slice.

The mean crystalline thickness of the control sample (3.81 (SD: 0.28) nm in dentine and 1.94 (SD: 0.06) nm in enamel) is consistent with the earlier transmission electron microscopy (TEM) studies and XRD data (Marten et al., 2010; Reiche et al., 2002). The increase of mean crystalline thickness happened after 400 °C which implied the HAp crystallites starting to sinter, leading to grain size growth. This process becomes dramatic after 600 °C, as can be confirmed by tracking the WAXS peak variation as illustrated in the

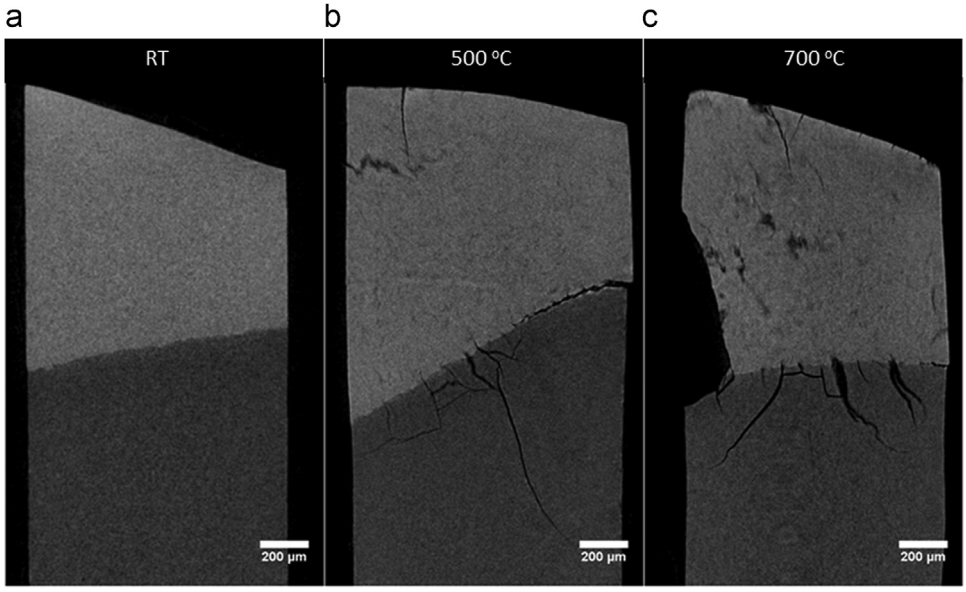

Fig. 6 – Crack development revealed by micro-CT cross-sectional images. The control sample (a) shows no cracks around the DEJ; whilst an increase in number of cracks and lifting of the enamel can be seen at 500 °C (b) and 700 °C (c).

Fig. 5 (Pramanik et al., 2013). In addition, the small increase in crystallite size for enamel with increasing temperature is likely to be related to the denser arrangement of HAp crystallites compared with dentine.

4.1.2. *Orientation and degree of alignment*

The local structural variation of the degree of alignment in dentine with distance from DEJ (Fig. 3b) represents an internal ultra- and micro-structural adaptation matching the geometry of the human tooth. The higher degree of alignment of HAp crystallites near DEJ is expected to stiffen the dentine. Thus the higher mineral particle co-alignments beneath the chewing surface cusps may be important for the transfer or the redistribution of mastication loads from the much harder, highly mineralised enamel deep into bulk dentine (Eliceiri et al., 2012).

The degree of alignment in dentine (0.23 (SD: 0.03)) from the control sample (room temperature, Fig. 4c and d) shows an almost random orientation of HAp crystallites, while the result in enamel indicates a stronger textured orientation (0.50 (SD: 0.02)). This is consistent with earlier SAXS results for dental tissue (Eliceiri et al., 2012; Jiang et al., 2005), where the internal architecture in dentine was observed to be net-like fibrils wound around tubules with decorated HAp crystallites. If it is observed along tubule direction, the fibrils will display an almost random distribution (Bozec et al., 2005). Therefore, when the beam illuminates perpendicular to the dental slice, i.e. perpendicular to the cross section of tubule, the HAp crystallites will have a much lower degree of alignment than that of well-packed HAp crystallites in enamel, which crystallites partially aligned along the prisms (or rods) (Macho et al., 2003). It is noted that in both dentine and enamel, there is a reduction in the degree of alignment as the temperature increased. The reduction of the overall degree of alignment as well as the bump gradient of the central line observed in Fig. 3b with increasing temperature may be explained by the burning-off or gradual disappearance of the organic phase most of which is collagen. Since the organic phase serves as the support of the structure, such disappearance may lead to the rearrangement of crystallites associated with rotation or anisotropic sintering. In addition, the rearrangement of crystallites may increase the crystal perfection, especially in dentine (Fig. 5), due to its larger amount of organic phase than in enamel.

4.2. *Mechanical properties characterization*

Both hardness and reduced modulus mapping showed the obvious contrast of properties between the dentine and enamel. The boundary between dentine and enamel is clearly shown in Fig. 2j–o and regions with large reduced modulus and hardness match very well as expected. However, it was found that the transition feature of mechanical properties in dentine was not as clear as the ultrastructural visualization, which was partly due to the low resolution of nanoindentation compared with SAXS/WAXS and the mechanical-response dispersion of both enamel and dentine. In addition, the existing cracks or surface defects in all the samples may affect the indentation results, and increase the relatively large error bounds in Fig. 4.

The hardness (0.7 (SD: 0.1) GPa in dentine and 3.0 (SD: 1.3) GPa in enamel) and reduced modulus (20 (SD: 6) GPa in dentine and 70 (SD: 17) GPa in enamel) of the control sample were consistent with the earlier nanoindentation studies on dental tissues (Roy and Basu, 2008; Tesch et al., 2001). The different behaviours of dentine and enamel might result from their different mineral contents. The initial reduction of the mechanical properties in dentine might be due to the gradual disappearance of collagen and the subsequent increase at higher temperatures might be explained by the occurrence of sintering and significantly increased crystal perfection, which

was partly reflected in the sharper peak variation in dentine in Fig. 5.

4.3. *Ultrastructure and mechanical properties correlation*

The relationship between the variations of the ultrastructure and mechanical properties with respect to different temperatures are reflected in Fig. 4a–d. As illustrated in Fig. 4a and b, in the enamel the reduced modulus (solid black symbols) and hardness (solid blue symbols) decrease as the mean thickness (solid red symbols) goes up. Similar phenomenon can also be observed in the dentine as illustrated in the empty symbols. The bigger the mean crystalline thickness is, the lower the mechanical properties would be, as reported by Tesch et al. (Tesch et al., 2001). Thus, the mean thickness was found to be a good predictor of the reduced modulus and hardness.

No obvious correlation between the degree of alignment and the mechanical properties can be observed in Fig. 4c and d except that the region with higher modulus as shown in Fig. 2 almost matches the region with higher degree of alignment of HAp crystallites, which indicates that the local structural variation may result in the local change of modulus in the same area. Furthermore, the distribution of the orientation of HAp crystallites may indicate a correlation between the orientation effect or texture effect and the mechanical property variation, as discussed in our previous work (Sui et al., 2013; Sui et al., 2014).

The consistent tendency of reduced modulus and hardness (Bao et al., 2004) is observed in Fig. 4. The observed alteration of the mechanical properties within the dental slice as the temperature increases may facilitate the crack propagation, since the decrease of hardness indicates the reduction of the ultimate strength (Krishna et al., 2013), which is visible in micro-CT observation (see Fig. 6).

5. Conclusions

The effects of heat treatment on human dental tissues were successfully elucidated by a systematic study of the combined SAXS/WAXS mapping and nanoindentation mapping techniques. Quantitative analysis of SAXS patterns of human teeth samples revealed a temperature-dependent variation of the mean thickness and the degree of alignment of nanoscale mineral phase (HAp crystallites) both in dentine and enamel. Furthermore, nanoindentation mapping captured the remarkable decrease of the hardness and modulus as the temperature increased. The relationship between the ultrastructural changes and mechanical behaviour changes with increasing temperature indicates that the structure has a strong effect on the mechanical properties.

In conclusion, the combination of synchrotron-based SAXS/WAXS and nanoindentation mapping methods has been shown to be a powerful method for the determination of the variation of the structural–mechanical property relationship in human dental tissues induced by the thermal treatment. Ultimately, the SAXS mapping approach developed in the present study might allow further design and optimization of laser treatment strategies for clinical applications, and will possibly provide an effective approach to deduce the heating history for teeth samples in the forensic and archaeological context.

Acknowledgements

AMK acknowledges the support of EPSRC through grants EP/I020691 “Multi-disciplinary Centre for In-situ Processing Studies (CIPS)”, EP/G004676 “Micromechanical Modelling and Experimentation”, and EP/H003215 “New Dimensions of Engineering Science at Large Facilities”. Diamond Light Source is acknowledged for providing the beam time.

REFERENCES

Al-Jawad, M., Steuwer, A., Kilcoyne, S.H., Shore, R.C., Cywinski, R., Wood, D.J., 2007. 2D mapping of texture and lattice parameters of dental enamel. Biomaterials 28, 2908–2914.

Angker, L., Swain, M.V., Kilpatrick, N., 2005. Characterising the micro-mechanical behaviour of the carious dentine of primary teeth using nano-indentation. J. Biomech. 38, 1535–1542.

Bao, Y.W., Wang, W., Zhou, Y.C., 2004. Investigation of the relationship between elastic modulus and hardness based on depth-sensing indentation measurements. Acta Mater. 52, 5397–5404.

Beckett, S., Rogers, K.D., Clement, J.G., 2011. Inter-species variation in bone Mineral behavior upon heating. J. Forensic Sci. 56, 571–579.

Bozec, L., de Groot, J., Odlyha, M., Nicholls, B., Nesbitt, S., Flanagan, A., Horton, M., 2005. Atomic force microscopy of collagen structure in bone and dentine revealed by osteoclastic resorption. Ultramicroscopy 105, 79–89.

Bragg, W.H., Bragg, W.L., 1933. The Crystalline State, Vol. 1. A General Survey Bell, London.

Daniels, J.E., Pontoni, D., Hoo, R.P., Honkimaki, V., 2010. Simultaneous small- and wide-angle scattering at high X-ray energies. J. Synchrotron Radiat. 17, 473–478.

Deymier-Black, A.C., Almer, J.D., Stock, S.R., Haeffner, D.R., Dunand, D.C., 2010. Synchrotron X-ray diffraction study of load partitioning during elastic deformation of bovine dentin. Acta Biomater. 6, 2172–2180.

Ebenstein, D.M., Pruitt, L.A., 2006. Nanoindentation of biological materials. Nano Today 1, 26–33.

Eliceiri, K.W., Berthold, M.R., Goldberg, I.G., Ibanez, L., Manjunath, B.S., Martone, M.E., Murphy, R.F., Peng, H., Plant, A.L., Roysam, B., Stuurmann, N., Swedlow, J.R., Tomancak, P., Carpenter, A.E., 2012. Biological imaging software tools. Nat. Methods 9, 697–710.

Enzo, S., Bazzoni, M., Mazzarello, V., Piga, G., Bandiera, P., Melis, P., 2007. A study by thermal treatment and X-ray powder diffraction on burnt fragmented bones from tombs II, IV and IX belonging to the hypogeic necropolis of “Sa Figu” near Ittiri, Sassari (Sardinia, Italy). J. Archaeol. Sci. 34, 1731–1737.

Fong, H., Sarikaya, M., White, S.N., Snead, M.L., 2000. Nano-mechanical properties profiles across dentin-enamel junction of human incisor teeth. Mater. Sci. Eng. C-Biomimetic Supramol. Syst. 7, 119–128.

Fratzl, P., Schreiber, S., Boyde, A., 1996. Characterization of bone Miner. crystals in horse radius by small-angle X-ray scattering. Calcif. Tissue Int. 58, 341–346.

Fried, D., Zuerlein, M.J., Le, C.Q., Featherstone, J.D.B., 2002. Thermal and chemical modification of dentin by 9–11-mu m CO_2 laser pulses of 5–100-mu s duration. Lasers Surg. Med. 31, 275–282.

Hammersley, A.P. 1997. "FIT2D: An Introduction and Overview" ESRF Internal Report.
Haque, F., 2003. Application of nanoindentation to development of biomedical materials. Surf. Eng. 19, 255–268.
He, L.H., Swain, M.V., 2009. Enamel—A functionally graded natural coating. J. Dentistry 37, 596–603.
Hiller, J.C., Thompson, T.J., Evison, M.P., Chamberlain, A.T., Wess, T.J., 2003. Bone Mineral change during experimental heating: an X-ray scattering investigation. Biomaterials 24, 5091–5097.
Hsu, C.M., Lin, A.D., Chien, H.L., Hung, T.P., Kuang, J.H., Using nanoindentation techniques to investigate the Young's moduli for human teeth of different ages.
Jacobs, H.R., Thompson, R.E., Brown, W.S., 1973. Heat-transfer in teeth. J. Dent. Res. 52, 248–252.
Jiang, H.D., Liu, X.Y., Lim, C.T., Hsu, C.Y., 2005. Ordering of self-assembled nanobiominerals in correlation to mechanical properties of hard tissues. Appl. Phys. Lett., 86.
Kinney, J.H., Marshall, S.J., Marshall, G.W., 2003. The mechanical properties of human dentin: a critical review and re-evaluation of the dental literature. Crit. Rev. Oral Biol. Med. 14, 13–29.
Krishna, S.C., Gangwar, N.K., Jha, A.K., Pant, B., 2013. On the prediction of strength from hardness for copper alloys. J. Mater. 2013, 1–6.
Kugler, M., 2003. X-ray diffraction analysis in forensic science: the last resort in many criminal cases. Adv. X-ray Anal., 46.
Le Bourhis, E., Patriarche, G., 2007. TEM-nanoindentation studies of semiconducting structures. Micron 38, 377–389.
Le Bourhis, E., Patriarche, G., Largeau, L., Riviere, J.P., 2004. Polarity-induced changes in the nanoindentation response of GaAs. J. Mater. Res. 19, 131–136.
Lim, C.T., Hairul Nizam, B.R., Omar, B.H.B., Chng, H.K., Yap, A.U.J., 2005. Probing the nanomechanical properties of teeth. ICF11 proceeding.
Macho, G.A., Jiang, Y., Spears, I.R., 2003. Enamel microstructure–a truly three-dimensional structure. J. Human Evol. 45, 81–90.
Marshall, G.W., Balooch, M., Gallagher, R.R., Gansky, S.A., Marshall, S.J., 2001. Mechanical properties of the dentinoenamel junction: AFM studies of nanohardness, elastic modulus, and fracture. J. Biomed. Mater. Res. 54, 87–95.
Marshall, S.J., Balooch, M., Breunig, T., Kinney, J.H., Tomsia, A.P., Inai, N., Watanabe, L.G., Wu-Magidi, I.C., Marshall, G.W., 1998. Human dentin and the dentin–resin adhesive interface. Acta Mater. 46, 2529–2539.
Marten, A., Fratzl, P., Paris, O., Zaslansky, P., 2010. On the Miner. in collagen of human crown dentine. Biomaterials 31, 5479–5490.
Oliver, W.C., Pharr, G.M., 1992. An Improved technique for determining hardness and elastic-modulus using load and displacement sensing indentation experiments. J. Mater. Res. 7, 1564–1583.
Patriarche, G., Le Bourhis, E., Khayyat, M.M.O., Chaudhri, M.M., 2004. Indentation-induced crystallization and phase transformation of amorphous germanium. J. Appl. Phys. 96, 1464–1468.
Piga, G., Malgosa, A., Thompson, T.J.U., Enzo, S., 2008. A new calibration of the XRD technique for the study of Archaeological burned human remains. J. Archaeol. Sci. 35, 2171–2178.
Piga, G., Thompson, T.J.U., Malgosa, A., Enzo, S., 2009. The potential of X-Ray diffraction in the analysis of burned remains from forensic contexts. J. Forensic Sci. 54, 534–539.
Piga, G., Solinas, G., Thompson, T.J.U., Brunetti, A., Malgosa, A., Enzo, S., 2013. Is X-ray diffraction able to distinguish between animal and human bones?. J. Archaeol. Sci. 40, 778–785.
Pramanik, S., Hanif, A.S.M., Pingguan-Murphy, B., Abu Osman, N.A., 2013. Morphological change of heat treated bovine bone: a comparative study. Materials 6, 65–75.
Reiche, I., Vignaud, C., Menu, M., 2002. The crystallinity of ancient bone and dentine: new insights by transmission electron microscopy. Archaeometry 44, 447–459.
Rinnerthaler, S., Roschger, P., Jakob, H.F., Nader, A., Klaushofer, K., Fratzl, P., 1999. Scanning small angle X-ray scattering analysis of human bone sections. Calcif. Tissue Int. 64, 422–429.
Rogers, K., Beckett, S., Kuhn, S., Chamberlain, A., Clement, J., 2010. Contrasting the crystallinity indicators of heated and diagenetically altered bone Mineral. Palaeogeogr. Palaeoclimatol. Palaeoecol. 296, 125–129.
Rogers, K.D., Daniels, P., 2002. An X-ray diffraction study of the effects of heat treatment on bone mineral microstructure. Biomaterials 23, 2577–2585.
Roy, S., Basu, B., 2008. Mechanical and tribological characterization of human tooth. Mater. Charact. 59, 747–756.
Shipman, P., Foster, G., Schoeninger, M., 1984. Burnt bones and teeth—an experimental-study of color, morphology, crystal-structure and shrinkage. J. Archaeol. Sci. 11, 307–325.
Sui, T., Sandholzer, M.A., Baimpas, N., Dolbnya, I.P., Walmsley, A.D., Lumley, P.J., Landini, G., Korsunsky, A.M., 2013. Multi-scale modelling and diffraction-based characterization of elastic behaviour of human dentine. Acta Biomater. 9, 7937–7947.
Sui, T., Lunt, A.J., Baimpas, N., Sandholzer, M.A., Hu, J., Dolbnya, I.P., Landini, G., Korsunsky, A.M., 2014. Hierarchical modelling of in situ elastic deformation of human enamel based on photoelastic and diffraction analysis of stresses and strains. Acta Biomater. 10, 343–354.
Ten Cate, A.R., 1998. Oral histology: development, structure, and function, 5th Ed. Mosby, St. Louis, Mo., London.
Tesch, W., Eidelman, N., Roschger, P., Goldenberg, F., Klaushofer, K., Fratzl, P., 2001. Graded microstructure and mechanical properties of human crown dentin. Calcif. Tissue Int. 69, 147–157.
Tesch, W., Vandenbos, T., Roschgr, P., Fratzl-Zelman, N., Klaushofer, K., Beertsen, W., Fratzl, P., 2003. Orientation of mineral crystallites and mineral density during skeletal development in mice deficient in tissue nonspecific alkaline phosphatase. J. Bone Miner. Res. 18, 117–125.
Thompson, T.J.U., 2005. Heat-induced dimensional changes in bone and their consequences for forensic anthropology. J. Forensic Sci. 50, 1008–1015.
Thompson, T.J.U., Islam, M., Bonniere, M., 2013. A new statistical approach for determining the crystallinity of heat-altered bone Miner. from FTIR spectra. J. Archaeol. Sci. 40, 416–422.
Thompson, T.J.U., Islam, M., Piduru, K., Marcel, A., 2011. An investigation into the internal and external variables acting on crystallinity index using Fourier Transform Infrared Spectroscopy on unaltered and burned bone. Palaeogeogr. Palaeoclimatol. Palaeoecol. 299, 168–174.
Zuerlein, M.J., Fried, D., Featherstone, J.D.B., 1999. Modeling the modification depth of carbon dioxide laser-treated dental enamel. Lasers in Surg. Med. 25, 335–347.